

Modeling Effects of Adding a Flux  
Channel to a Planar Magnet-Coil Actuator

by

Jacob Bourgeois

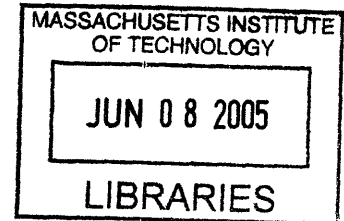
Submitted to the Department of Mechanical  
Engineering in Partial Fulfillment  
of the Requirements for the Degree of

B.S. Mechanical Engineering

at the

Massachusetts Institute of Technology

May 2005 [June 2005]



© 2005 Jacob D. Bourgeois.  
All rights reserved.

The author hereby grants to MIT permission to reproduce and to distribute publicly paper  
and electronic copies of this thesis document in whole or in part.

Signature of Author.....

A handwritten signature in black ink, appearing to read "J. Bourgeois".

Jacob D. Bourgeois  
Department of Mechanical Engineering  
May 6, 2005

Certified by.....

A handwritten signature in black ink, appearing to read "Martin Culpepper".

Martin Culpepper  
Rockwell International Assistant Professor of Mechanical Engineering  
Thesis Supervisor

Accepted by.....

Ernest G. Cravalho  
Chairman, Undergraduate Thesis Committee

**ARCHIVES**

Modeling Effects of Adding a Flux  
Channel to a Planar Magnet-Coil Actuator

by

Jacob D. Bourgeois

Submitted to the Department of Mechanical Engineering  
on May 6, 2005 in partial fulfillment of the  
requirements for the Degree of Master of Science in  
Mechanical Engineering

ABSTRACT

Planar magnet-coil actuators are used in many different MEMS devices. This report describes one way to improve the actuator range per current input of planar coil actuators. This is accomplished by adding a flux channel around and beneath the actuator's magnet. The Lorentz force is created by putting a current carrying planar coil over a magnet in an actuator assembly. The Lorentz force depends on the current vector and the magnetic field vector. In this thesis the Lorentz force is altered by changing the direction and concentration of the magnetic field.

Magnetic fields may be modeled as flux lines traveling from the north face of the magnet to the south face along the least resistant path. Iron is a magnetic material with 4000 times the magnetic permeability of air, so when iron is placed in a magnetic field, the majority of the magnetic flux will travel from North to South through the iron. This "channel" alters the way the magnetic field would normally travel given the bare magnet.

The magnetic flux that travels through the channel depends in part upon the channel geometry. The result of varying the width of this channel is modeled and tested in this work. The physical principle was examined in simulations by varying channel width and then extracting the corresponding actuator output. A relationship was fit to the simulated results. The actuator output augmentation was maximized at a critical width and remained steady thereafter. Beyond the critical width, the addition of the flux channel was able to produce more than 45% increase in the actuator force. Experimental results showed less than a 5% difference from the simulated results.

Thesis Supervisor: Martin Culpepper

Title: Rockwell International Assistant Professor of Mechanical Engineering

<b>Table of Contents</b>	
<b>ABSTRACT</b> .....	<b>2</b>
<b>Table of Contents</b> .....	<b>3</b>
<b>Table of Figures</b> .....	<b>4</b>
<b>Chapter 1: Introduction</b> .....	<b>6</b>
<b>Chapter 1: Introduction</b> .....	<b>6</b>
<b>1.1 Concept and terms defined</b> .....	<b>6</b>
1.2 Background .....	7
<b>1.3 Motivation</b> .....	<b>7</b>
<b>1.4 Proposed solution</b> .....	<b>8</b>
<b>Chapter 2: Physics and Theory</b> .....	<b>9</b>
<b>2.1 Mechanical system</b> .....	<b>9</b>
<b>2.2 Electro-magnetic system</b> .....	<b>10</b>
<b>2.3 Complete system theory</b> .....	<b>12</b>
<b>Chapter 3: Simulations and modeling</b> .....	<b>13</b>
<b>3.1 Electro-magnetic simulations</b> .....	<b>13</b>
<b>3.2 Finite element analysis</b> .....	<b>15</b>
<b>3.3 System simulation</b> .....	<b>16</b>
<b>Chapter 4: Case study design</b> .....	<b>20</b>
<b>4.1 Channel</b> .....	<b>20</b>
<b>4.2 Flexure</b> .....	<b>20</b>
<b>4.3 Coil layout</b> .....	<b>21</b>
<b>4.4 Assembly design</b> .....	<b>22</b>
<b>Chapter 5: Experiment</b> .....	<b>25</b>
<b>5.1 Part synthesis</b> .....	<b>25</b>
<b>5.2 Tolerances</b> .....	<b>28</b>
<b>5.3 Part assembly</b> .....	<b>29</b>
<b>5.4 Experiment set-up</b> .....	<b>29</b>
<b>5.5 Experimental procedure</b> .....	<b>30</b>
<b>Chapter 6: Results: analysis and discussion</b> .....	<b>32</b>
<b>6.1 Experimental results</b> .....	<b>32</b>
<b>6.2 Simulation vs. experiment comparison</b> .....	<b>33</b>
<b>6.3 Sources of error</b> .....	<b>35</b>
<b>Chapter 7: Conclusions</b> .....	<b>37</b>
<b>7.1 Purpose</b> .....	<b>37</b>
<b>7.2 Solution</b> .....	<b>37</b>
<b>7.3 Validity of solution</b> .....	<b>37</b>
<b>Chapter 8: References</b> .....	<b>38</b>
<b>Appendix</b> .....	<b>39</b>
<b>A.1 Force vs. current simulations</b> .....	<b>39</b>
<b>A.2 Experimental results</b> .....	<b>40</b>

## Table of Figures

<b>FIGURE 1:</b> Cross-section of a planar magnet-coil actuator.....	6
<b>FIGURE 2:</b> This force vs. current curve shows the benefit of adding a flux channel to the actuator assembly.....	7
<b>FIGURE 3:</b> Top view of the mechanical component as designed and used in this analysis.....	9
<b>FIGURE 4:</b> Magnetic flux lines as simulated without a flux channel.....	11
<b>FIGURE 5:</b> Magnetic flux lines as simulated in the presence of a flux channel, where $t$ and $w$ are the channel base thickness and channel width respectively.....	11
<b>FIGURE 6:</b> Free body diagram of the actuator.....	12
<b>FIGURE 7:</b> Simulated results for force vs. channel width for current of 1A and constant channel base thickness.....	14
<b>FIGURE 8:</b> Force vs. current simulation for channel width of 3.18mm.....	15
<b>FIGURE 9:</b> FEA simulation which shows exaggerated deflection of actuator.....	16
<b>FIGURE 10:</b> Displacement vs. force from FEA simulation of final flexure design.....	17
<b>FIGURE 11:</b> Combined simulation data that shows deflection vs. current for 3.18mm channel width.....	18
<b>FIGURE 12:</b> Displacement vs. channel width for simulated results at input current of 1A.....	18
<b>FIGURE 13:</b> Curve fit for simulation results of deflection vs. width at 1A.....	19
<b>FIGURE 14:</b> Cross-section view of channel rotated about axis of symmetry that shows the channel width, thickness and radius labeled.....	20
<b>FIGURE 15:</b> Bottom view of the flexure assembly.....	21
<b>FIGURE 16:</b> Spiral coil where leads are connection points to the current source, $R_{coil}$ is the coil radius and $N$ is the number of turns.....	22
<b>FIGURE 17:</b> Half-view cross-section of the coil layout .....	22
<b>FIGURE 18:</b> Exploded view of the solid modeled assembly.....	23
<b>FIGURE 19:</b> Final assembly model.....	23
<b>FIGURE 20:</b> PC Board Kit with marker, etchant solution, and solvent labeled used for etching coil layout. ....	25
<b>FIGURE 21:</b> Close-up of the coil layout after being cut out and taped to flexure assembly.....	26
<b>FIGURE 22:</b> The 9.53mm channel ring (left) and the channel base (right) .....	27
<b>FIGURE 23:</b> The three different channel rings of widths 3.18mm, 6.35mm and 9.53mm from left to right.....	28
<b>FIGURE 24:</b> Final system assembly of the machined housing, spacer, flexures, and capacitance probe mount.....	29
<b>FIGURE 25:</b> Experimental set-up.....	30
<b>FIGURE 26:</b> System flow diagram and the corresponding interactions as labeled.....	31
<b>FIGURE 27:</b> Deflection vs. current for the four experimental runs.....	32
<b>FIGURE 28:</b> Experimental results with anticipated no channel case.....	33
<b>FIGURE 29:</b> Deflection vs. current for channel width of 6.35mm for both the experimental and the simulated results.....	34
<b>FIGURE 30:</b> Deflection per current ratio vs. channel width, given a channel base thickness of 2.7mm.....	34

# Chapter 1: Introduction

## 1.1 Concept and terms defined

The goal of this thesis is to improve the force output of a planar magnet-coil actuator for a given current input. A planar magnet-coil actuator, shown in Figure 1, consists of a planar coil attached to a flexure suspended above a cylindrical magnet. A flexure connects the output platform to a rigid base.

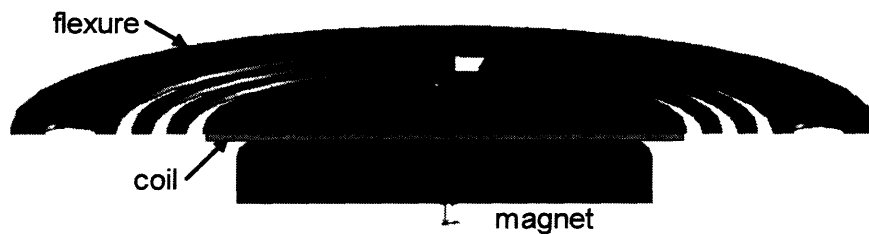


**FIGURE 1:** Cross-section of a planar magnet-coil actuator

The actuator range is increased by adding a flux channel. The flux channel is a magnetically conductive component that encases the magnet on all sides except for the north face of the magnet. The channel provides a less resistive path to magnetic flow. This new path changes the direction and concentration of the field. Figure 2 shows that the force output for a given set of input currents is greater for the actuator with a flux channel than the actuator with a bare magnet [01].

<b>FIGURE 31:</b> Force vs. the height of the coil above the magnet for constant current and channel parameters.....	36
<b>FIGURE 32:</b> Force vs. current for channel width of 6.35mm.....	39
<b>FIGURE 33:</b> Force vs. current for channel width for 9.53mm.....	40
<b>FIGURE 34:</b> Deflection vs. current for 3.18mm and 0mm channel widths.....	41
<b>FIGURE 35:</b> Deflection vs. current for channel width of 9.53mm.....	41
<b>FIGURE 36:</b> Deflection vs. current for channel width of 0mm but with a 2.7mm channel base thickness.....	42
<b>FIGURE 37:</b> Deflection vs. current for the channel width of 6.35mm.....	42

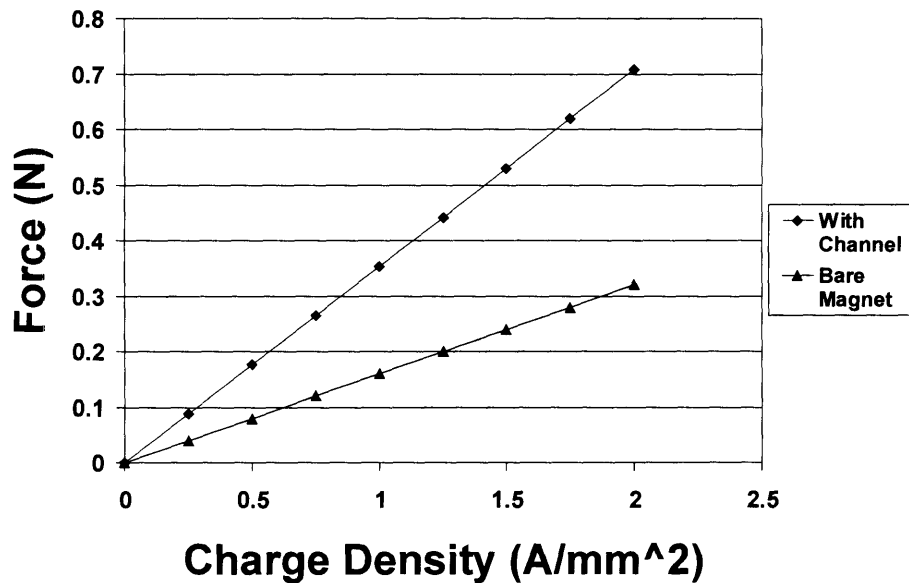


**FIGURE 2:** This force vs. current curve shows the benefit of adding a flux channel to the actuator assembly

### 1.2 Background

The addition of a flux channel to improve actuator output has been documented before. Kim et al. display similar graph as in Figure 2 that shows the qualitative improvement obtained by adding a flux channel [02]. Their work stops there, leaving much to be known about how to quantify the increase in force and whether or not there is a way to optimize the improvement by varying channel geometries.

### 1.3 Motivation

Micro-Electro-Mechanical Systems or MEMS are micro-scale mechanical systems that contain sensors, actuators and electronics, on a common silicon substrate. With a growing desire for pocket size devices, the applications for MEMS devices are increasing. The current application fields range from BioTech to gaming controllers.

The MEMS design being studied in this paper is the actuator, which can be used in things like sensors, scanners, accelerometers, and speakers. One example of MEMS application in speakers is in hearing aids, where a sound amplification system is needed to fit in a person's ear. An actuator in the hearing aid takes electrical energy to move a membrane or flexure in order to maximize the volume change in the speaker box. The greater the volume change or membrane deflection, the better or louder the sound created. This is just one example of many systems like it which care to increase output force for a given input current.

#### **1.4 Proposed solution**

The need of augmenting the output force for a given magnetic field strength and input current is met by manipulating the magnetic field direction. By adding a ferro-magnetic flux channel beneath and beside the magnet in the actuator, the relative B-field flowing through the coil and the corresponding Lorentz force can be increased. This work looks at the force as a function of the channel geometry and looks to characterize the channel in terms of the channel width and base thickness associated with it.

This paper will give an overview of the physics working in the system. The system model will be set up and the software used to create simulations will be described. Then the design of the case study will be looked at and the reasons for setting up the experiment. Following this will be the experimental procedures, results and analysis. Then, the system model and simulated results will be compared to the experimental results and a conclusion will be drawn about the channels usefulness and the usefulness of the model.



# Chapter 2: Physics and Theory

This chapter will discuss the underlying principles that govern the performance of the actuator. The chapter is broken into two parts, (1) a section on the mechanical component and (2) a section on the electro-magnetic component. The complete system will then be analyzed to determine a relationship for the actuator behavior.

## 2.1 Mechanical system

The mechanical component is a monolithic component that consists of a stage, an outer mounting ring and flexures that connect them. The flexure, pictured in Figure 3, is designed to have a specific stiffness.

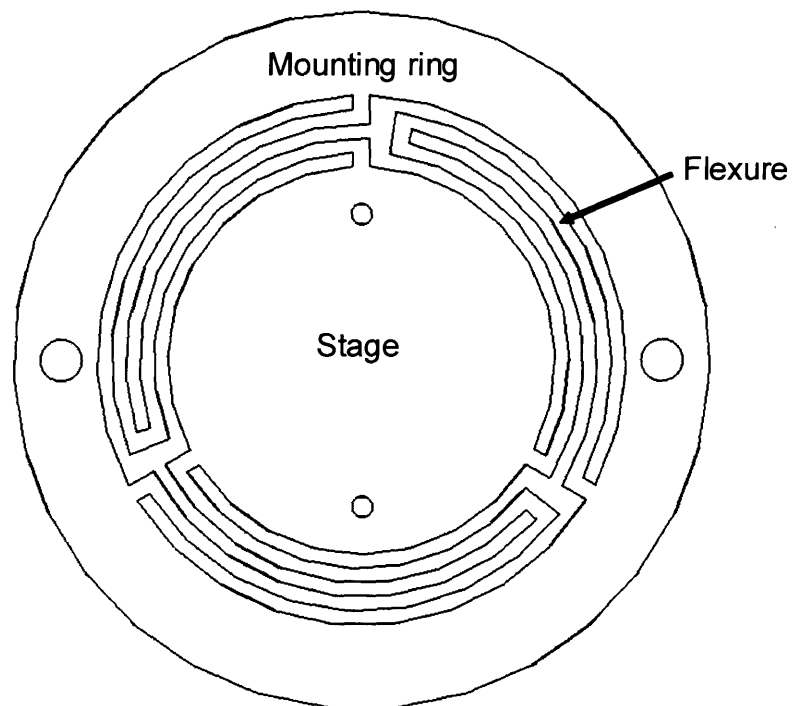


**FIGURE 3:** Top view of the mechanical component as designed and used in this analysis

Figure 3 shows the three main components to the flexure, the mounting ring, the stage and the flexure beams. The mounting ring, for the purposes of the analysis and the experiment, will be held in a fixed position. All forces applied to the system will act upon the stage.

That deflection as a function of force of cantilever beams is given by Equation 1.

$$\delta = (FL^3) / (3EI) \tag{1}$$

where  $\delta$  is the deflection,  $F$  is the force applied to the stage which can be modeled as the tip of the flexure beams,  $L$  is the length of the flexure beams,  $E$  is the elastic modulus, and  $I$  is the moment of inertia.

Modeling the flexure as a cantilever beam is only an approximation. The exact form of Equation 1 for the flexure is difficult to derive due to its complex geometry. For the beams in this work, a force applied to the stage produces axial twisting, linear bending and rotational deformation in different segments of the flexure beams. In addition, the length,  $L$ , in Equation 1 corresponds to a straight beam [04].

A simplification of Equation 1 modeling the geometric parameters as a stiffness coefficient allows us to use the spring equation. The spring constant was evaluated using a simulation. This will be covered in Chapter 3. The spring is related to the applied force using Equation 2.

$$\delta = (1/k) \times F \quad (2)$$

where,  $k$  is the spring constant (or beam stiffness),  $F$  is the applied force from the electro-magnetic component, and  $\delta$  is the deflection.

## 2.2 Electro-magnetic system

The Lorentz force is calculated via Equation 3.

$$F_{Lorentz} = I \times B \quad (3)$$

where  $I$  is the magnitude of the current through the wire, and  $B$  is the magnetic field vector. The seemingly simple equation is rather complex when non-straight conductor paths are used. In addition, the use of a flux channel results in complex magnetic fields. Calculating the cross product of  $I$  and  $B$  becomes a non-trivial exercise [07].

The component of the field line that is horizontal when flowing through the planar coil is the one which will create a resultant force in the  $z$ -direction. The other components cancel out due to symmetry about the coil's axis of symmetry, e.g. the  $z$  axis.

Figures 4 and 5 provide a comparison of the magnetic field lines in a half-space, cross-section of an actuator without and with a flux channel. The magnet, coil and field lines are rotationally symmetric about the axis of symmetry. The figures show the magnetic flux lines from the magnet in the presence of a flux channel and without it. Notice how the directions of the flux lines in Figure 5 are more horizontal when flowing through the coil. Figure 5 also shows the important flux channel parameters for this paper. The channel's base thickness,  $t$ , and the channel width,  $w$ , are labeled.

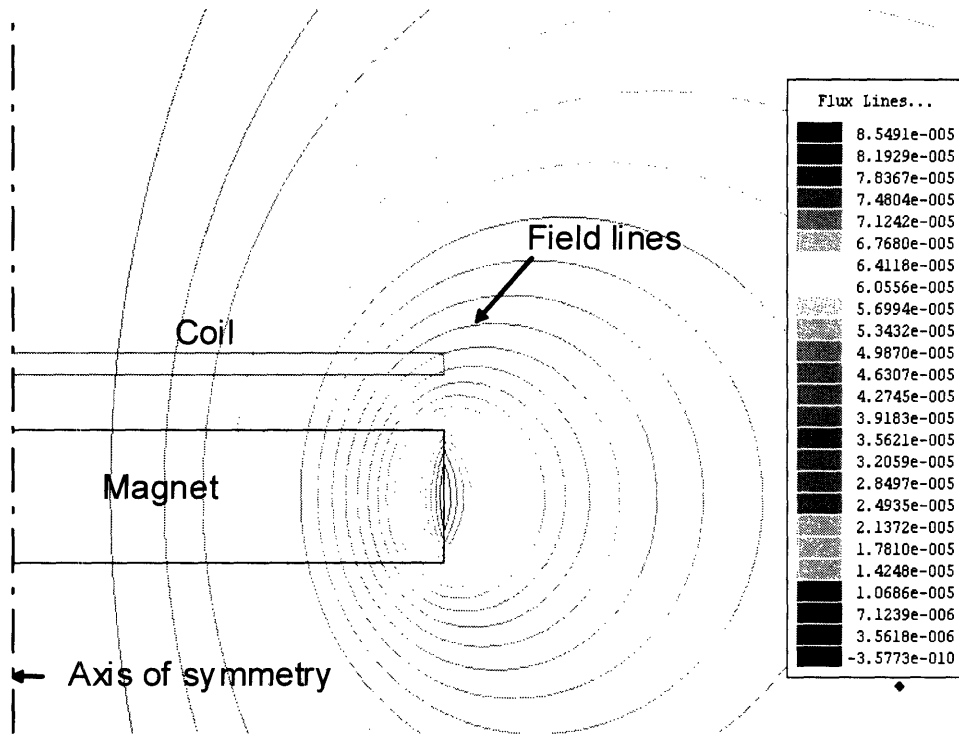


FIGURE 4: Magnetic flux lines as simulated without a flux channel.

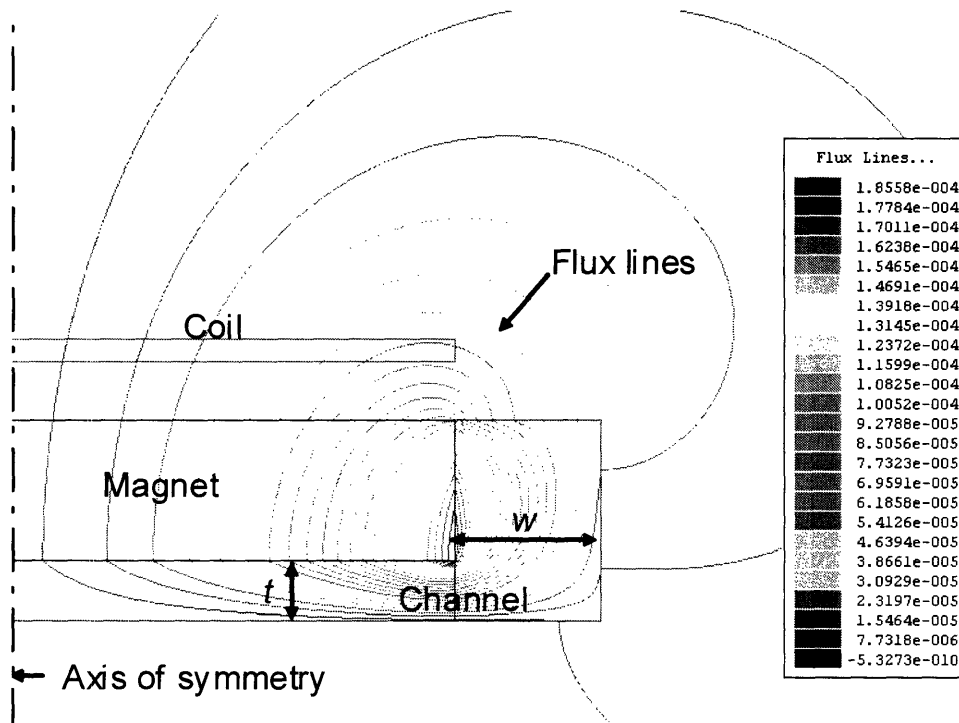
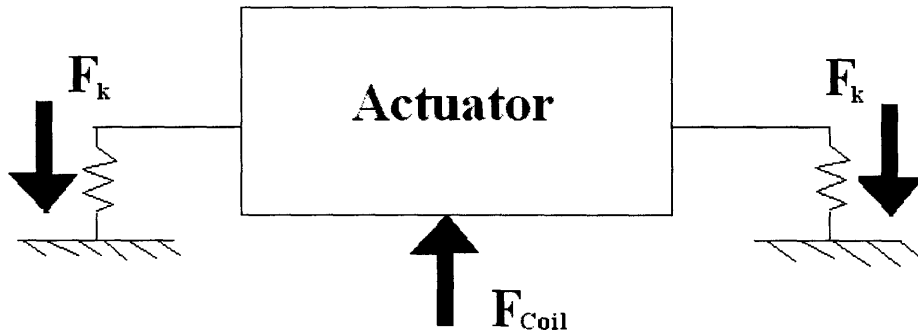


FIGURE 5: Magnetic flux lines as simulated in the presence of a flux channel, where  $t$  and  $w$  are the channel base thickness and channel width respectively.

### 2.3 Complete system theory

The system model may be created by combining the models of the Lorentz force and the spring force. The Lorentz force creates a positive force in the z-direction when current is run through the coil, and the flexure will offer a resistive force in the opposite direction. There will be an equilibrium deflection which changes as the current through the coil changes. Figure 6 shows a free body diagram of the actuator.



**FIGURE 6:** Free body diagram of the actuator

In Figure 6,  $F_k$  is the spring force from the flexure beams, and  $F_{coil}$  is the Lorentz force due to the magnet-coil interaction. The net force from the flexure beams may be modeled as one force so that the net spring force must be equal to the force from the coil when displacement settles to a finite deflection. At static equilibrium, the forces are equal as shown in Equation 4.

$$F_k = F_{coil} \quad (4)$$

When Equation 4 is combined with the definition of the spring force in Equation (2), and the Lorentz force in Equation (3) it simplifies to Equation 5.

$$\delta = (1/k) \times (I \times B) \quad (5)$$

# Chapter 3: Simulations and modeling

The simulations may be broken into two separate models, one for the mechanical component and one for the electro-magnetic component. The simulations of the individual components make it possible to develop a simulation for the entire actuator.

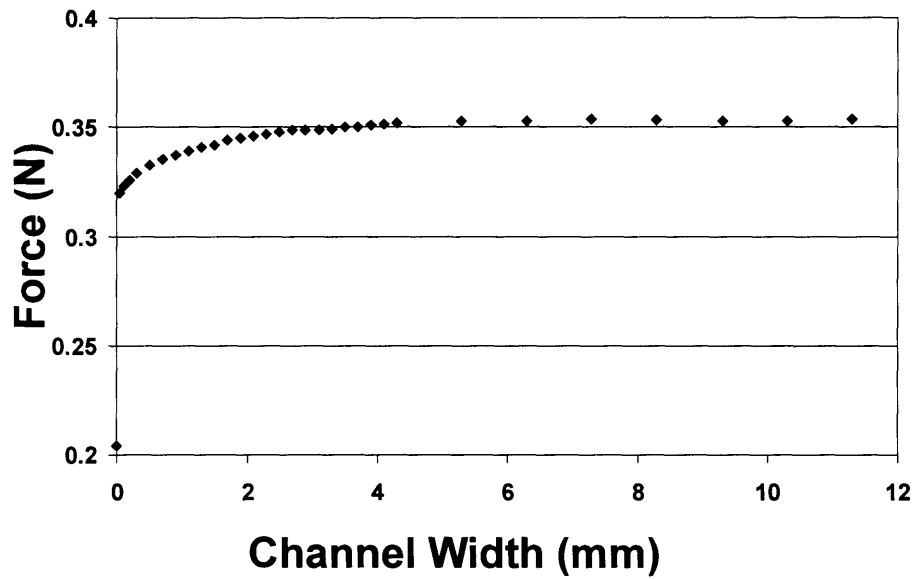
## 3.1 Electro-magnetic simulations

Ansoft's Maxwell SV was used to simulate the electro-magnetic characteristics of the actuator. The simulations were run in order to obtain data which reflects the effect of varying channel parameters and current in the coil. The coil carrying the current was modeled as a thin solid with a specific current. This approximation is quite good because the charges in a coil would be nearly evenly spread.

Maxwell SV is limited in that it can only run one current condition and geometric condition at a time. Due to this limitation, each data point collected was for a separate simulation. While collecting each data point is fast for a short number of refinements (around 10), the percent error is so great that the data is not usable. As a result the system should be run to at least 27 refinements in order to reduce the error to less than 0.1%. Each run requires more time than the previous run because the elemental mesh is refined.

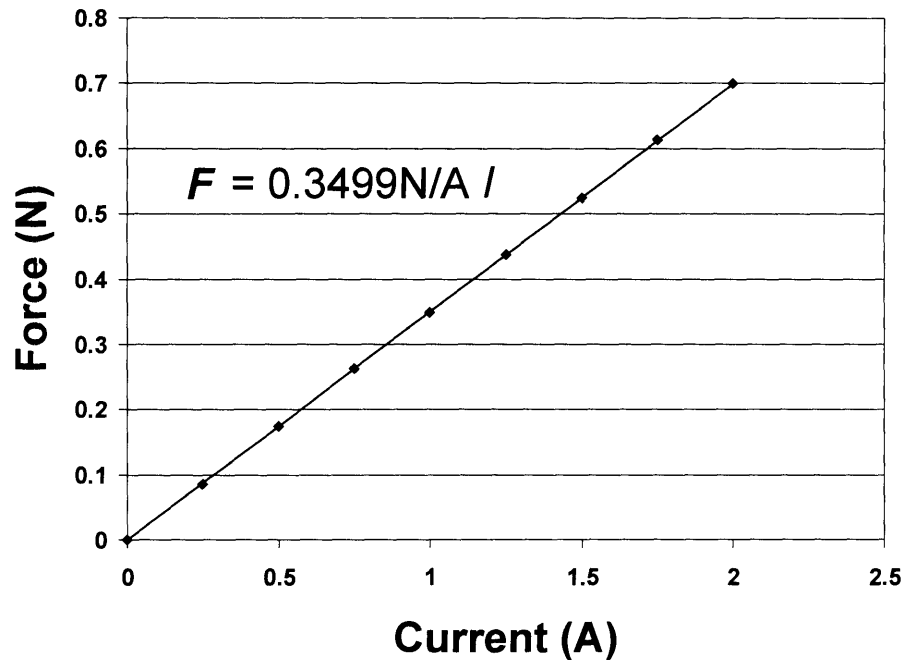
As such, in the future it is recommended to use more sophisticated software to model the simulation such as FEMLAB, which enables one to parameterize both geometry and current. Another benefit of using FEMLAB is its ability to run finite element analysis on the flexure in parallel with the Lorentz force simulations.

Figure 7 shows the output force associated with a varying channel width. In this figure, channel base thickness and current are held constant at 2.7mm and  $1\text{A/mm}^2$  respectively. The channel base is the channel encasing the bottom face of the magnet.



**FIGURE 7:** Simulated results for force vs. channel width for current of 1 A and constant channel base thickness.

Figure 7 shows an increase in force from 0.204 N to 0.320 N as one goes from a design with no flux channel to one which is 0.05 mm in width. Subsequent data points form a continuous curve that reaches a peak value at the critical channel width of 3.5 mm. Figure 8 shows the force output with varying input current.



**FIGURE 8:** Force vs. current simulation for channel width of 3.18mm

In the simulation in Figure 8, the channel width is set to 3.18mm. The channel base thickness remains 2.7mm, the same as in the previous simulation. Here we see that with a current varying from 0 to 2A, we have a force output linearly varying with current at 0.3499N/A. The charts for the other two channel widths are provided in the appendix.

### 3.2 Finite element analysis

The finite element analysis was run using CosmosWorks software. CosmosWorks like Ansoft, does not have the option of varying geometry in simulations. In FEMLAB this may be achieved using a MATLAB program file.

The force from the Maxwell simulation was used to set the flexure stiffness coefficient at a value which would yield the desired deflection. The flexure's stiffness was varied until an output deflection of 200 microns could be achieved with the force associated with the actuator channel geometry and an input current of 1A. The stiffness was varied by changing the characteristic length of the beam connectors. Figure 9 shows the final flexure in an exaggerated deflected state.

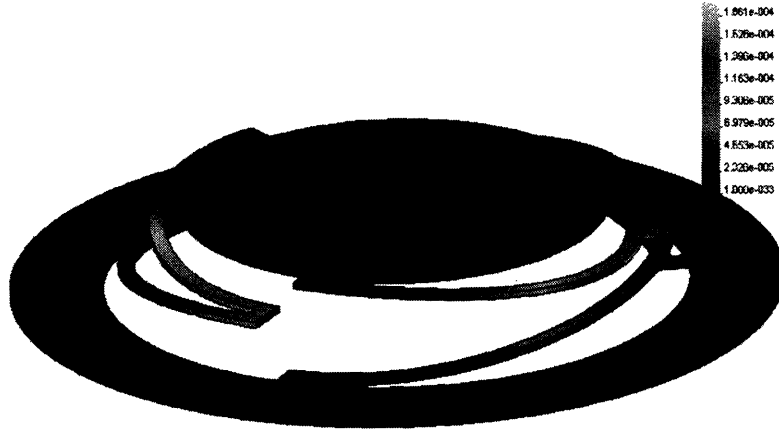


**FIGURE 9:** FEA Simulation which shows exaggerated deflection of actuator

Once the desired flexure stiffness was achieved, a set of simulations was run to get the deflection vs. force curve pictured in Figure 10. The beam stiffness was extracted off the curve to be 2.15 N/mm.

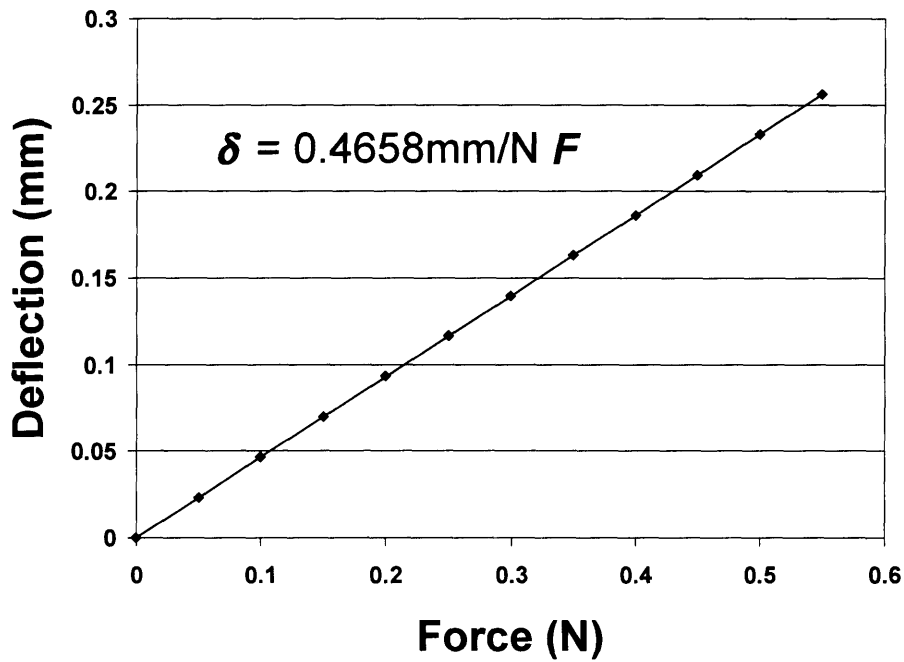


**FIGURE 10:** Displacement vs. force from FEA simulation of final flexure design

### 3.3 System simulation

The results from the simulations described in this section render the system model. The input force in the finite element analysis is the force output from the electro-magnetic



simulations. Substituting the electro-magnetic force into the FEA yields a relationship, pictured in Figure 11, between deflection and current.

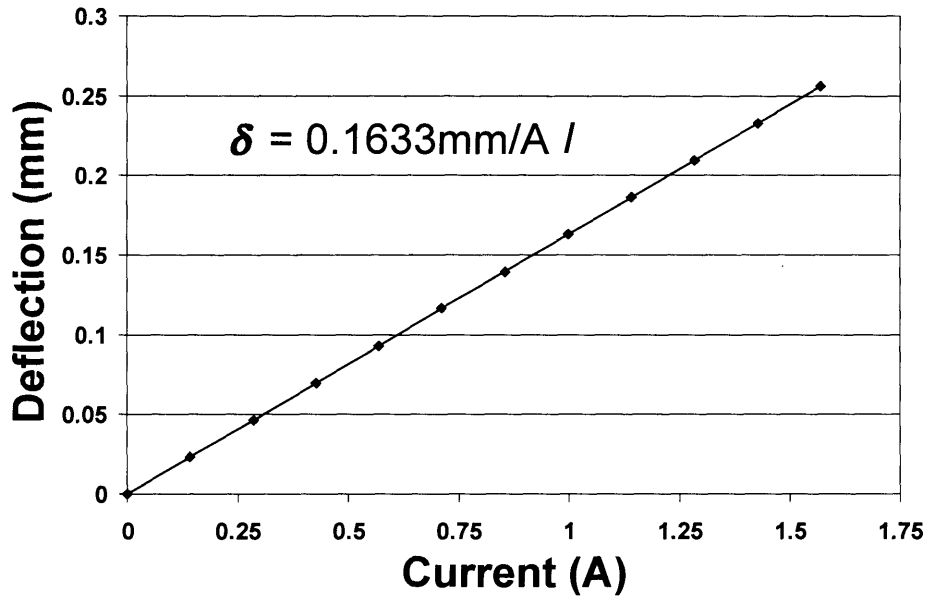


**FIGURE 11:** Combined simulation data that shows deflection vs. current for 3.18mm channel width.

We see in Figure 11 that there is a linear relation between the deflection and the current. This is expected due to the linear relationship of Lorentz and flexure forces. Further data was collected to determine the optimal channel width holding the base thickness constant. Figure 12 shows how the deflection of the actuator varies with the channel width.

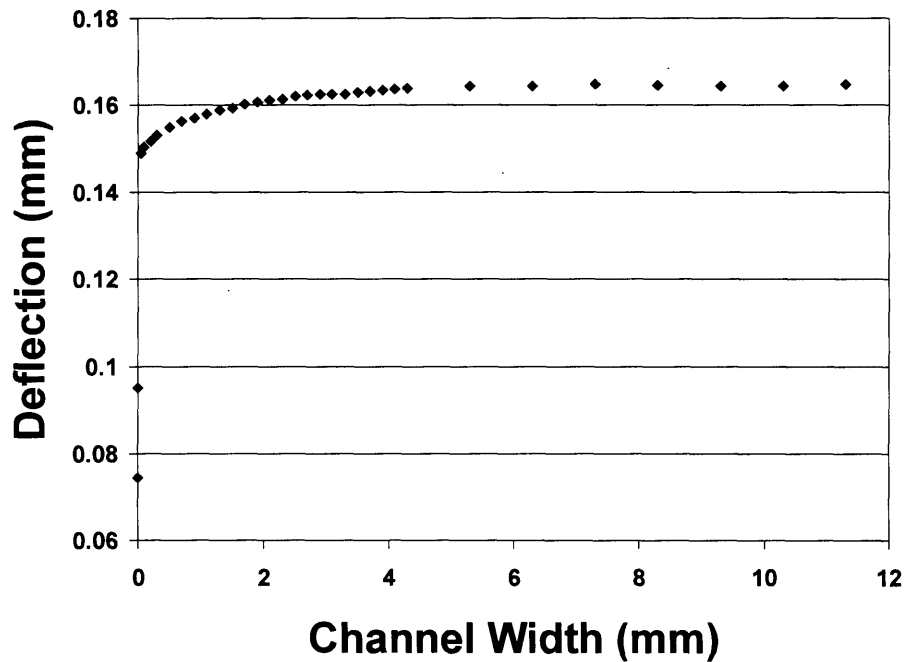


**FIGURE 12:** Displacement vs. channel width for simulated results at input current of 1A.

The change in force due to the change in width of the channel increases asymptotically. A width of 3.5mm is the critical width for which all of the magnetic flux may be routed through the channel without magnetic saturation. The final equation for deflection vs. current for the plot in Figure 11 is given in Equation 6.

$$\delta = 0.1633\text{mm}/A I \quad (6)$$

The relationship for the deflection vs. channel width is given in Equation 7.

$$\delta = 0.1478\text{mm} + 0.0102\text{mm} (1 - \exp(-2.6W/\text{mm})) \quad (7)$$

where  $W$  is the channel width in mm, and the numbers in the equation are for the curve fit values in Figure 13. These numbers were found by fitting a curve to a segment of the graph in Figure 12.

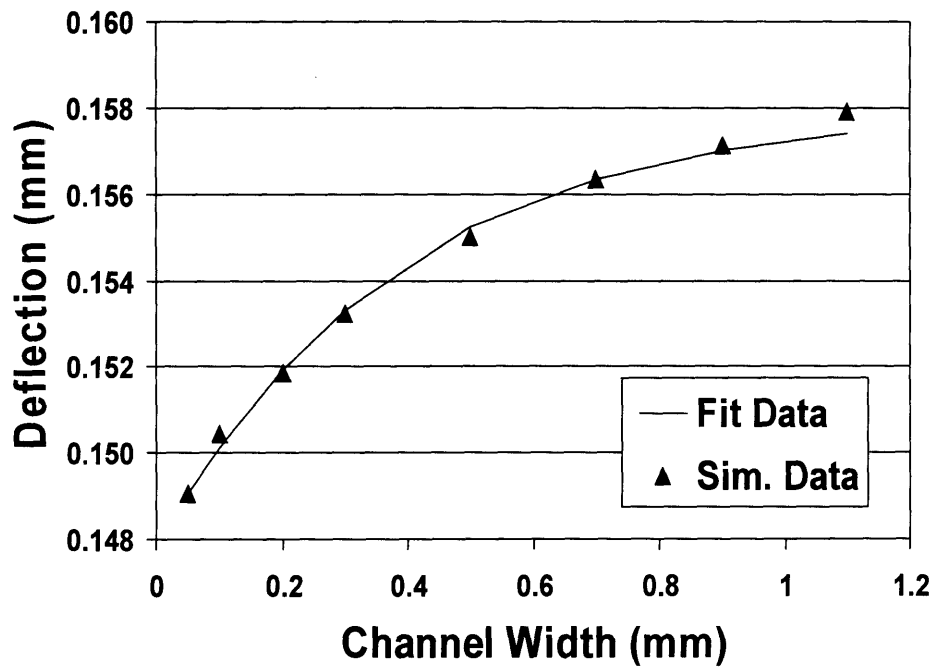


FIGURE 13: Curve fit for simulation results of deflection vs. width at 1A

# Chapter 4: Case study design

To verify this model a prototype was designed and tested to provide data for comparison with the model.

## 4.1 Channel

The channel was made up of two components, the inner channel base and the channel rings. Three channel rings with varying widths were used in the experiment. The base, as in the simulation, will be held constant at 2.7mm. This base thickness is larger than the critical thickness. Thicknesses that are smaller than the critical thickness limit the augmentation of actuator output due to saturation in the channel base. This thickness also holds the magnet an appropriate distance below the coil.

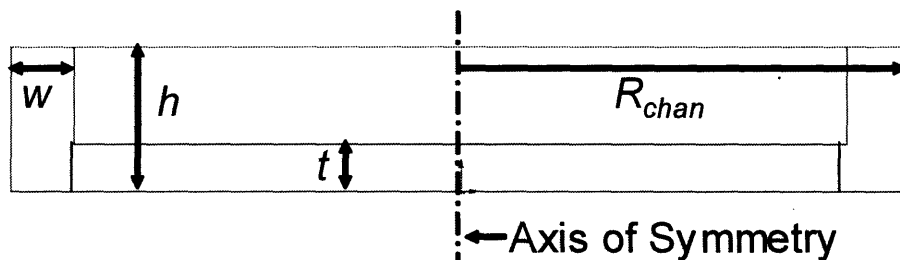


**FIGURE 14:** Cross-section view of channel (rotated about axis of symmetry) that shows the channel width, thickness and radius labeled

The channel base thickness was held constant at 2.7mm. The channel height was held constant at 8.9mm and level with the top of the magnet. The channel widths were 3.18mm, 6.35mm, and 9.53mm. These widths were chosen because they are big enough to machine easily and they cover much of the range of the simulated results.

## 4.2 Flexure

The flexures, as described in Chapter 2, were designed so the stage in the middle may be displaced the desired amount. Specifically it was desired to have deflections on the measurable range of the capacitance probe (200microns). The actuator was designed for z-axis deflection, but it can be twisted and rotated. This kind of deflection is undesirable in the analysis.

A second flexure was added to improve the resistance to twisting and rotation. This resistance came from separating the two flexures with a finite spacer. The spacer chosen was a hollow cylindrical aluminum channel separating the flexures by 12.7mm. This separation will eliminate all of the measurable twisting and force lost to bending moments. The hollow aluminum will be sturdy enough for uniform deflection and also light enough to remain negligible when compared to the spring forces resisting the

motion. The flexure assembly, pictured in Figure 15, was made by layering and attaching the two flexures and the spacer.

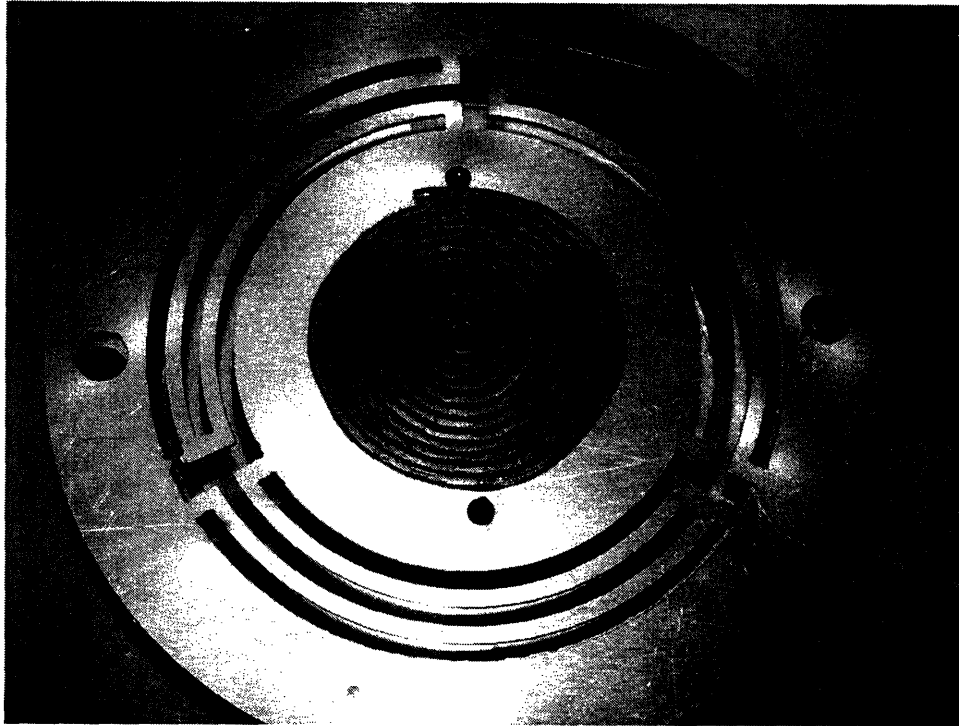


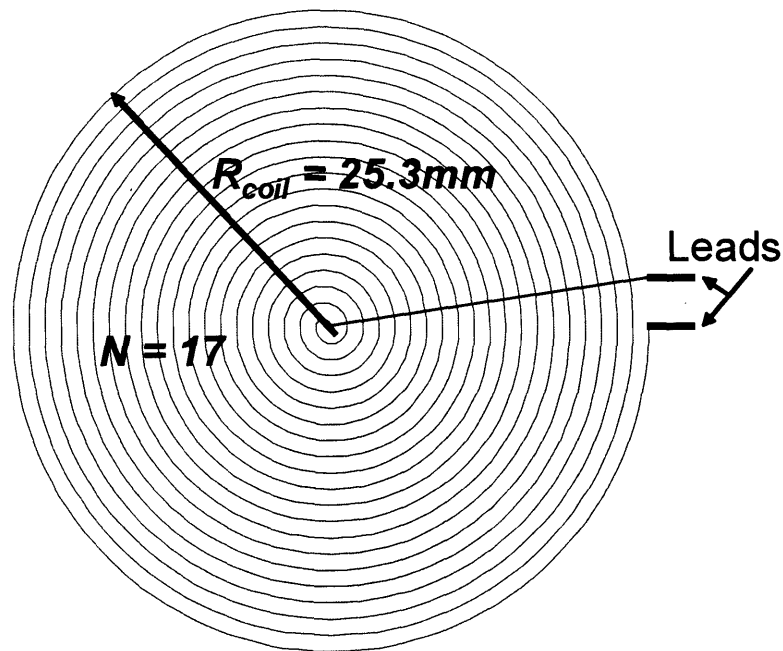
**FIGURE 15:** bottom view of the flexure assembly.

The combined beam stiffness,  $k_{net}$ , is equal to 2.15N/mm such that maximum deflections for inputs up to 2A are measurable by the capacitance probe.

#### **4.3 Coil layout**

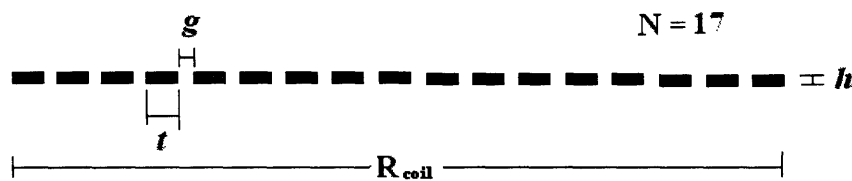
The coil layout, is just a simple spiral coil encompassing the whole area above the magnet, and not beyond. The magnetic field is shaped differently and has a different horizontal component magnitude at every position  $r$  away from the z-axis. A space of 0.3mm was left for space on either end of the 1.0mm coil width to minimize interference. The spiral contains 17 turns which sets the coil outside radius to that of the magnet.

Figure 16 shows the layout of the coil used in making the actual coil. This Figure shows the dimensions and important characteristics of the coil layout. The thickness,  $t$ , and the gap size,  $g$ , are not scaled to the actual design due to limitations in the software.



**FIGURE 16:** Spiral coil where leads are connection points to the current source,  $R_{coil}$  is the coil radius and  $N$  is the number of turns.

Figure 17 shows the cross-section of the coil. Figure 17 gives a better idea of what the important parameters of the coil are. The number of turns,  $N$ , is the most important parameter in the layout, because the net Amperes flowing through the cross section is what affects the force on the actuator. The coil height,  $h$ , the radius of the coil,  $R_{coil}$ , and the thickness,  $t$ , are important when relating to the modeled coil in the simulation.



**FIGURE 17:** Half-view cross-section of the coil layout

#### 4.4 Assembly design

The assembly, pictured in Figures 18 and 19, was designed so that the experiments could be run quickly and consistently. The housing was 12.7mm aluminum designed to hold the actuator and coil 3.66mm above the magnet. A space was machined out of the side for clearance for the wires carrying the current to the coil.

The capacitance probe mount was a modification of the clamp designed by Dariusz Golda in his experiment testing deflection of planar magnet-coil actuators [06]. Here a single capacitance probe was fit above the center of the flexure and held in place by a set

screw that tightens the clamp holding the probe. The capacitance probe mount is spaced 1.65mm above the flexure assembly by a simple ring spacer of sheet aluminum.

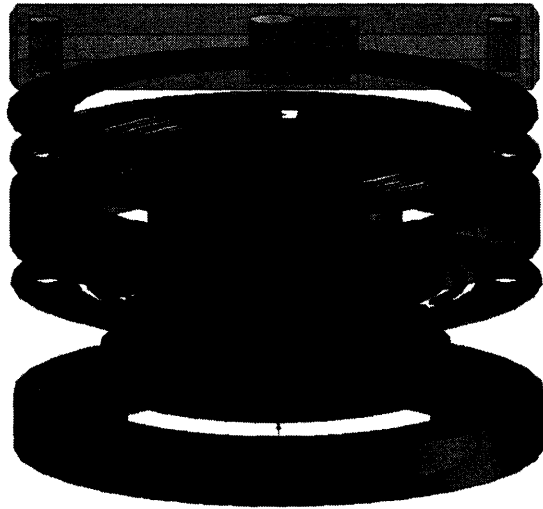


**FIGURE 18:** Exploded view of the solid modeled assembly

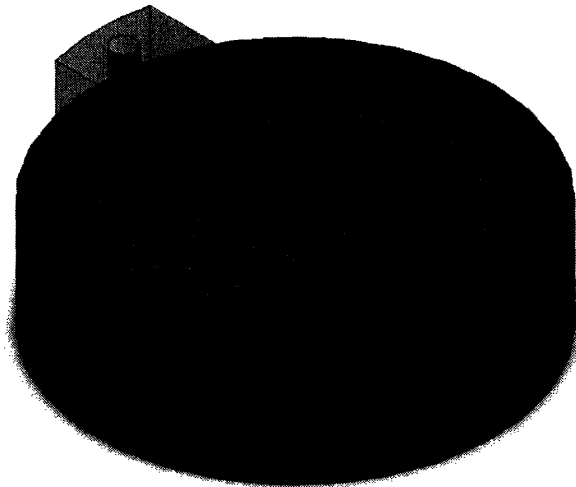


**FIGURE 19:** Final assembly model

The final assembly, pictured above in Figure 19, is small compact and sturdy. It offers enough assembly tolerance so that the system can be rebuilt easily. It is also sturdy enough such that if it were to be accidentally dropped the system would not be jeopardized. This will be useful packaging when the system is downsized to the micro-scale for MEMS applications.



# Chapter 5: Experiment

The experimental process was broken up into four main steps, part synthesis, assembly of the parts, set-up of the experiment, and the running of the experiment. This experiment allowed the testing of three different channel widths' deflections verses their corresponding current curves. The slopes of the corresponding graphs were extracted to give the overall advantage of the addition of the channel for all three channel widths. The experiment showed that the simulated results for actuator output as a function of width were correct.

## 5.1 Part synthesis

The parts for the experiment were made by waterjetting. Then they were post-machined on a Bridgeport milling machine to refine the specifications of design. The coil was created using the PC Board Kit, in Figure 20.

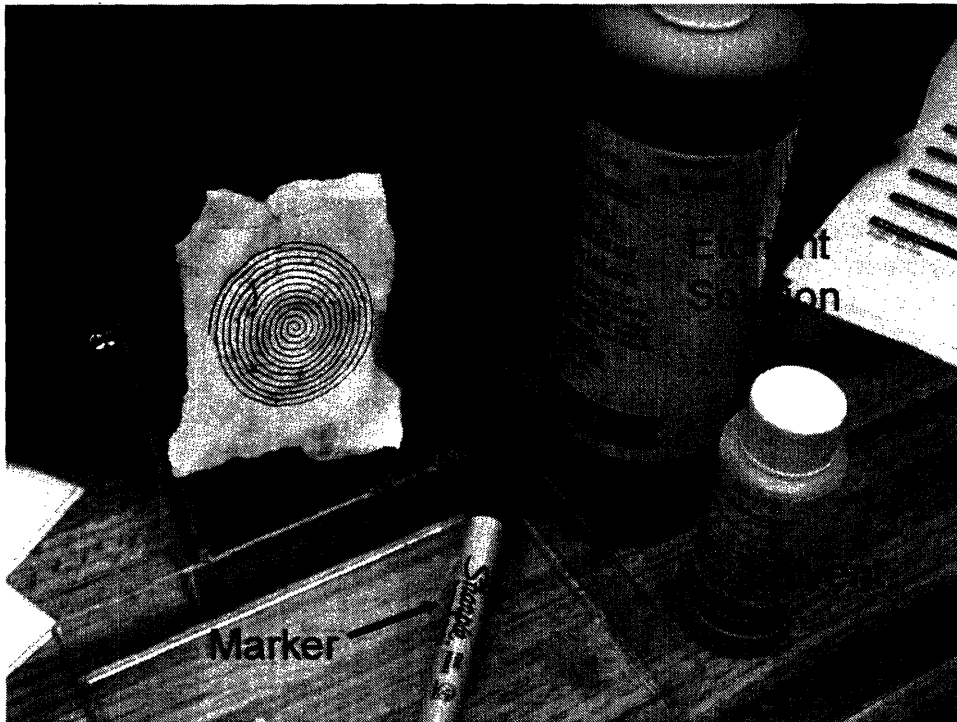


**FIGURE 20:** PC Board Kit with marker, etchant solution, and solvent labeled used for etching coil layout.

The PC Board Kit includes the Etchant solution, Etchant resistant marker, marker solvent, and bath for etching. The coil pictured in Figure 20 is the same as the one that was designed. The layout was copied onto the copper sheet then etched leaving the coil shown in Figure 21.



**FIGURE 21:** Close-up of the coil layout after being cut out and taped to flexure assembly.

The coil was cut out of the sheet and attached with double sided tape to the bottom of the flexure assembly. Pictured in Figure 22 are the channel parts. The base on the right in Figure 22 was fit inside the channel ring on the left to form a casing for the magnet.

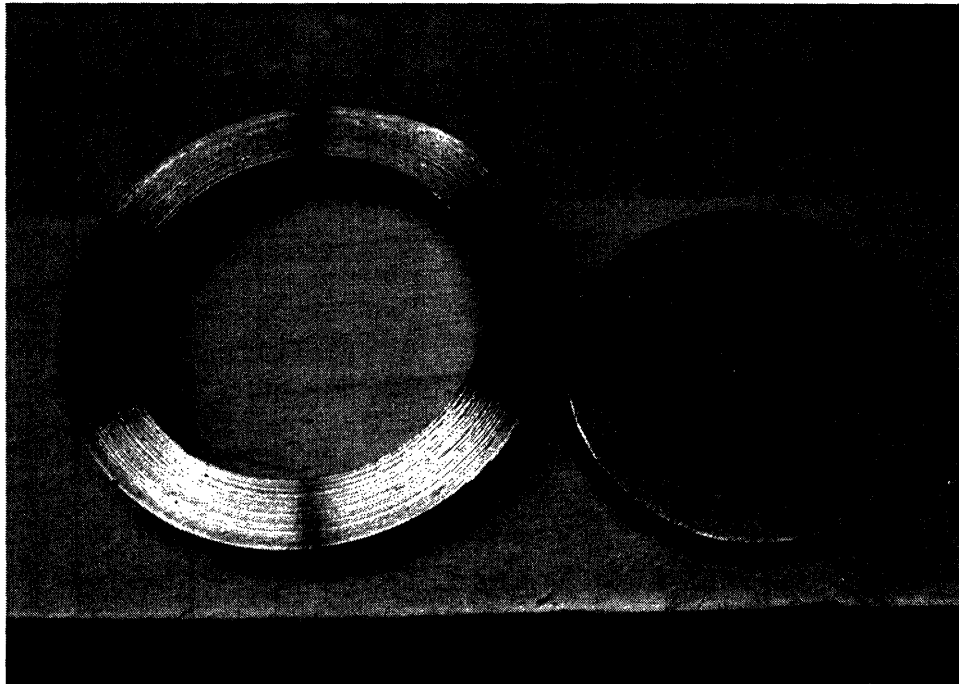


**FIGURE 22:** The 9.53mm channel ring (left) and the channel base (right)

The three channel rings were waterjetted and machined to slide easily around the magnet and base because of the strong magnetic forces that hold the assembled magnet and channel together. Figure 23 shows the three different channel widths which the magnet and base were fit into.

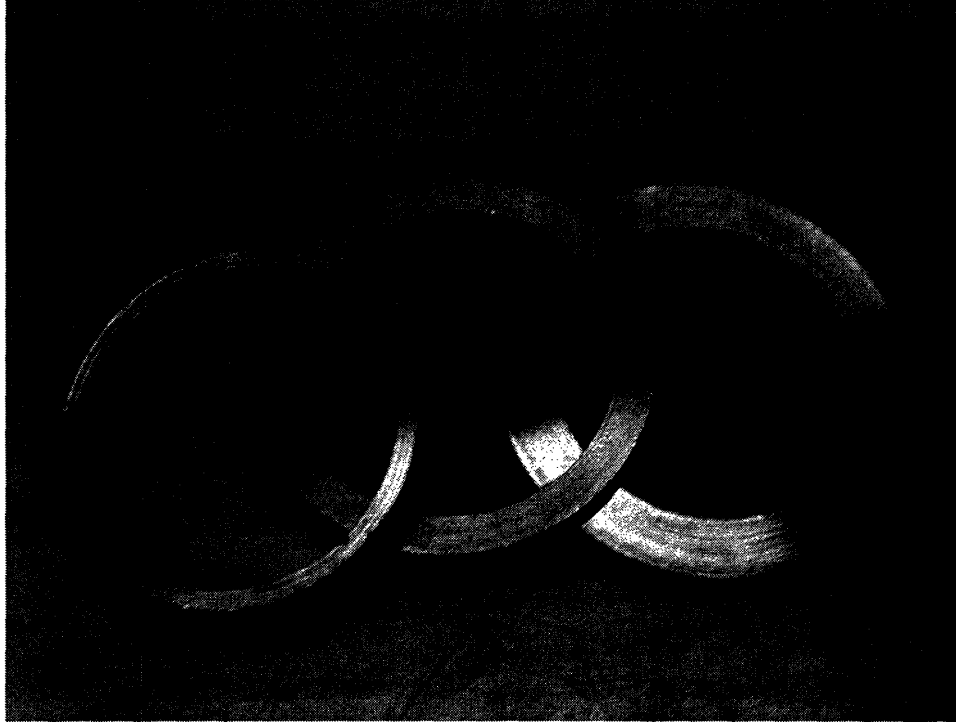


**FIGURE 23:** The three different channel rings of widths 3.18mm, 6.35mm and 9.53mm from left to right

## 5.2 Tolerances

The channels were made precise because of the magnet and base that were snugly fit into them. The waterjet left the channels with a finite slope on each edge. That slope was ground down so the magnet fit inside it. Each of the three channel rings were ground until a small clearance was left between the channel ring and the magnet to alleviate some of the difficulty of removing the magnet from the channel ring between each of the separate runs. This was different from our model, where the channel ring was designed to be exactly fit with both the magnet and the base.

Further, the channel base was not cut to the 2.7mm as specified. The difficulty of machining did not allow for this, so it was left at the original thickness of 3.18mm. Both 3.18mm and 2.7mm are above the critical base thickness for the channel so it did not affect the output deflection. The added base thickness was fit into the piece of aluminum, being used as a base, providing an added measure for positioning. The aluminum base was created to fix the assembly position.

The coil was designed to be 50.6mm in diameter (the magnet diameter) but because of the etching process a coil 38mm was created. Also the etching process limited the number of turns that could be drawn using the resistant pen, while leaving enough clearance between turns. The final coil layout in Figure 21 was used. The only effect this had on the results was the repositioning of the center of current across the cross section. The difference in radius does not affect the magnitude of the current because it was scaled due to the linear relation. So an incremental increase in current corresponded

to a like increase in displacement, and the relationship between the two was gathered, independent of actual current values.

### 5.3 Part assembly

As mentioned the coil was attached to the bottom of one of the flexures using two sided tape. The two flexures were glued to opposite ends of the spacer separating them. The flexure assembly was placed on top of the housing for support and to keep it the fixed distance above the magnet. The cap probe was mounted on top of the spacer which, in turn, was placed on top of the flexure assembly. The whole assembly, in Figure 24, was mounted on an aluminum plate that was included for its non-magnetic properties, for positioning the magnet and for anchoring the system together.

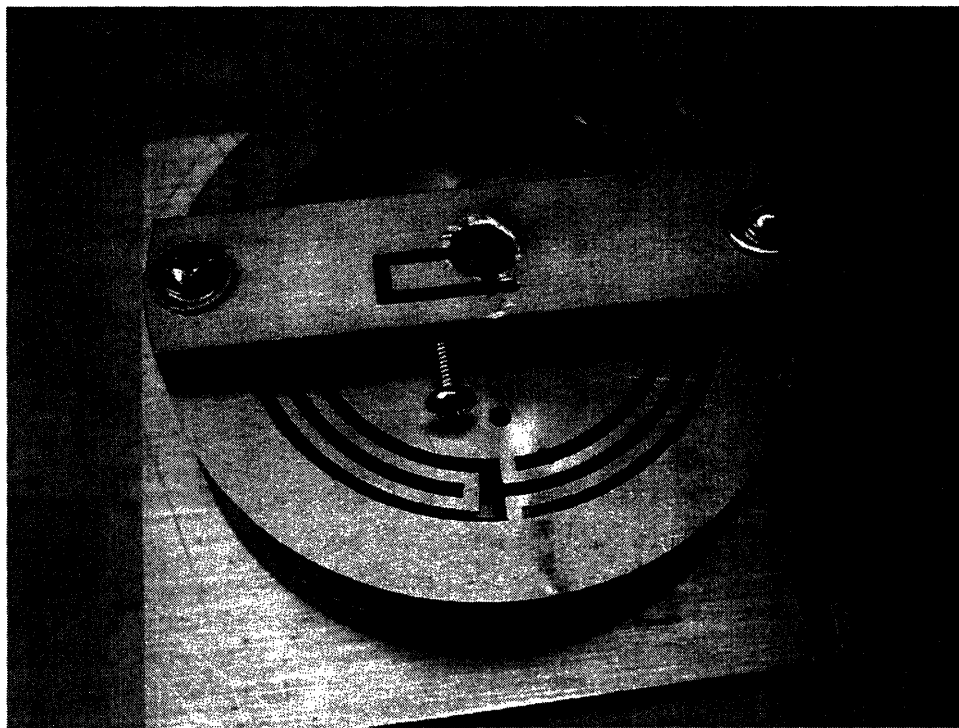


**FIGURE 24:** Final system assembly of the machined housing, spacer, flexures, and capacitance probe mount

### 5.4 Experiment set-up

The actual set-up of the experiment is shown in Figure 25. The black box in the upper right corner of the figure is the capacitance probe calibrator and power source. The white faced power source is the current input. Wires run from the current input to the coil in the assembly.



**FIGURE 25:** Experimental set-up

The capacitance probe was placed at an approximate height above the flexure assembly. A digital multi-meter was used to give a voltage output for deflection in the flexure.

### **5.5 Experimental procedure**

Figure 26 shows the flow diagram of the system. As outlined in Figure 26, the current was input from the current source to the planar coil. The Lorentz force on the flexure came from the constant B-field supplied by the magnet and the current flowing through the coil. The deflection of the actuator corresponding to the force from the coil was read by the capacitance probe, which was powered by the power supply. The capacitance probe sent a signal through the power supply to the digital multi-meter of the voltage associated with the deflection in the actuator.

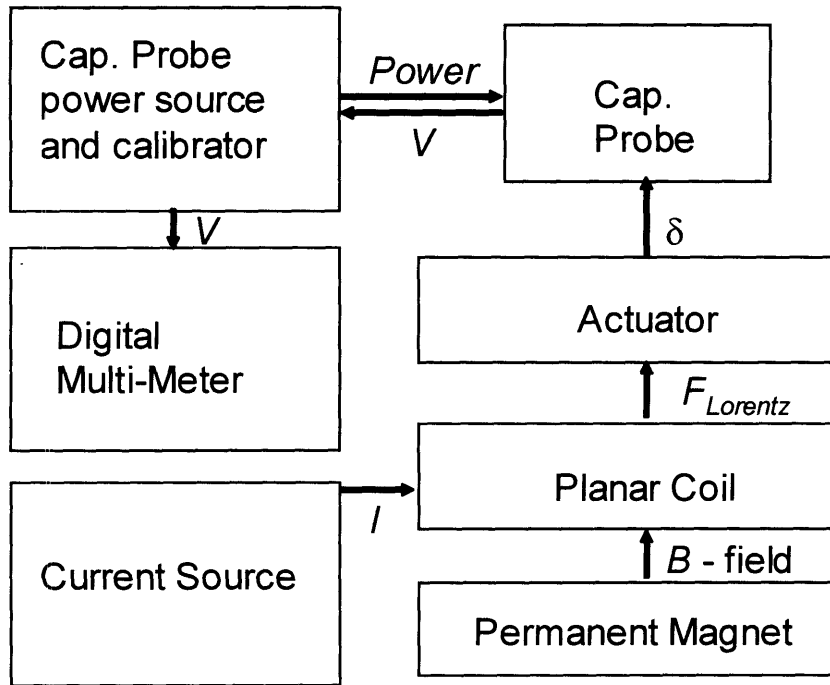


**FIGURE 26:** System flow diagram and the corresponding interactions as labeled

The output voltage was recorded and then turned into deflection with the given calibration relation of  $0.08 \text{ V}/\mu\text{m}$ . Then using a spreadsheet the deflections were plotted against the input current driving it.

# Chapter 6: Results: analysis and discussion

This chapter will outline the results gathered from the experiment, compare them to the suggested model, and discuss the similarities and differences between the two.

## 6.1 Experimental results

Figure 27 shows the experimental results for each of the channel widths. It was seen that the addition of any channel sizes adds force to the system. What is not clear from this Figure is the amount of channel necessary for optimal force output.

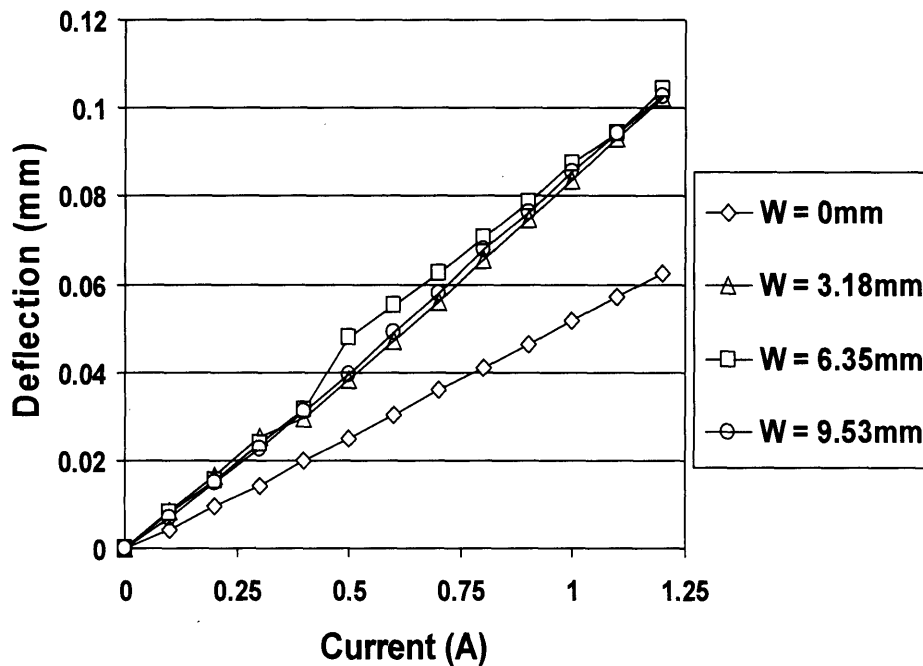


**FIGURE 27:** Deflection vs. Current for the four experiments run.

The channel ring of  $W = 0\text{mm}$  is appropriately labeled above in Figure 27 because the base thickness was left in place in order that the same distance from the coil could be maintained throughout all of the experiments. The simulated results show us that with the base thickness the force multiplier is  $0.204\text{ N/A}$ , and with the bare magnet the force multiplier is  $0.160\text{ N/A}$ . This tells us that the addition of the channel is even greater than what is pictured in Figure 27. Figure 28 models what the expected no channel run by using the conversion factor 78% of the data from the with channel base in place, giving us an approximate experimental value for the bare magnet case in Figure 28. The figure shows what would be the expected relationship based on the simulation results.



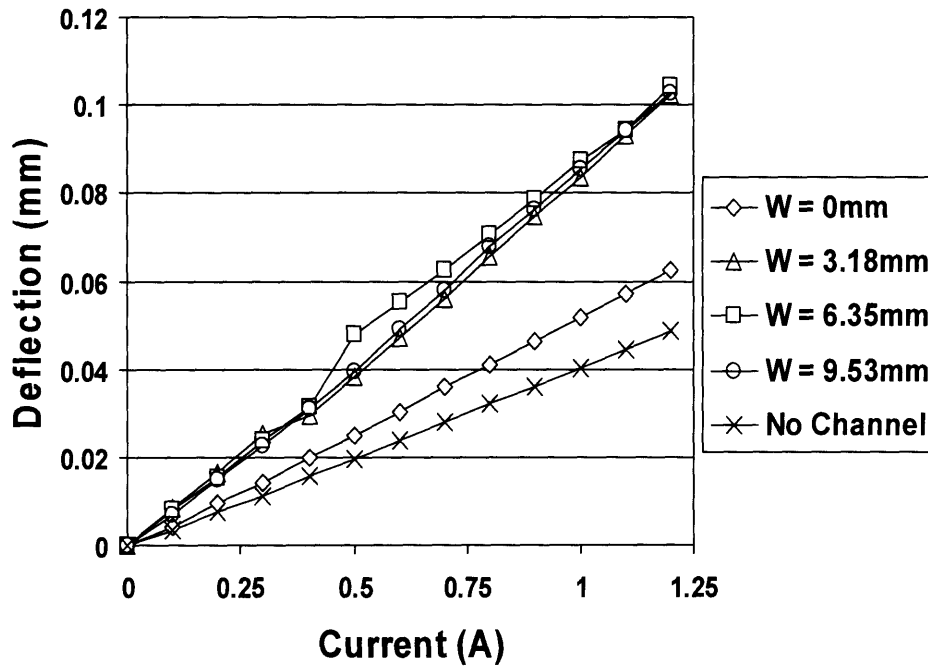


FIGURE 28: Experimental results with anticipated no channel case

### 6.2 Simulation vs. experiment comparison

Figure 29 shows the relationship between the experimental and simulated results. The experimental deflection vs. current multiplier was 26% of the expected simulated multiplier. This is a big discrepancy but the order of magnitude is the same, and with the sensitivity of the system described in the next section, the data is still useful in supporting the simulated model. What can be learned is the trend associated with the variance in channel width shown in Figure 30.

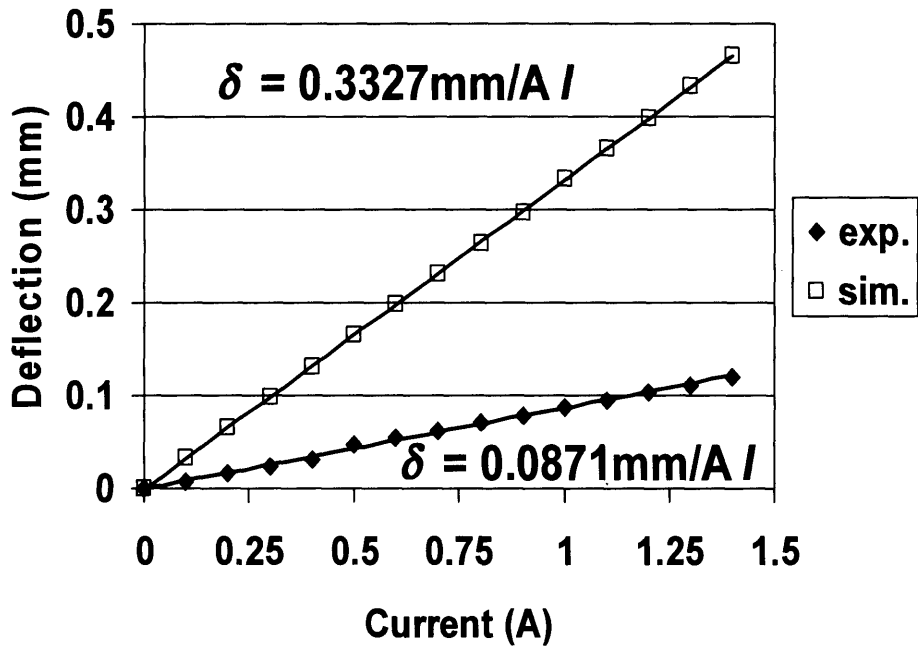


FIGURE 29: Deflection vs. current for channel width of 6.35mm for both the experimental and the simulated results

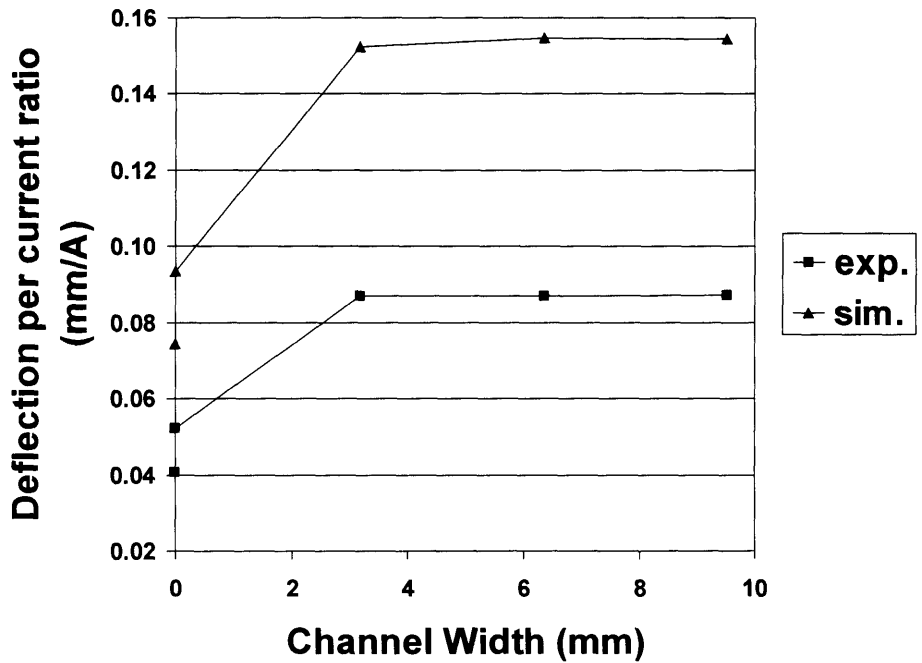


FIGURE 30: Deflection per current ratio vs. channel width, given an input current of 1A and a channel thickness of 2.7mm.

In Figure 30 the lowest deflection to current ratio on each of the two data series represents the bare magnet value, and the point directly above it corresponds to a channel width of 0mm but a base thickness of 2.7mm. The important thing to note from the two data series is that after a channel was added the force drastically increased.

In the experimental series in Figure 30, the addition of the channel corresponds to 46.7% increase in deflection. The increase from the simulated model gave a 48.8% increase in force. These results differ by 4.3%, which is small given the sensitivity of the experiment. The experiment agrees with the modeled amount of increase in actuator output due to adding a flux channel. The experimental relationship between width and actuator output also agrees with the model.

### **6.3 Sources of error**

One shortcoming of this experiment was the accuracy of the model of the spring stiffness of the flexures. When the two flexures were combined and epoxy was used to keep the spacer set between the two flexures, the spring constant could have been jeopardized. Through handling and manufacturing the flexures, the flexure beams might have been bent or worn. The spring constant could have been lower or higher depending on the way it was deformed. The quantity or percent error from this is not readily accessible without further tests. Further, during the experiment, the flexure could wear or sag from the continual loading and unloading of the flexure. Because of the flexure design the error associated with this should have been minimized.

The coil height is another important factor where slight variation could cause considerable error in the deflection measured. Figure 31 shows the variability in coil location. In the figure, current is held at 2A and channel geometry is held at constant width and base thickness.

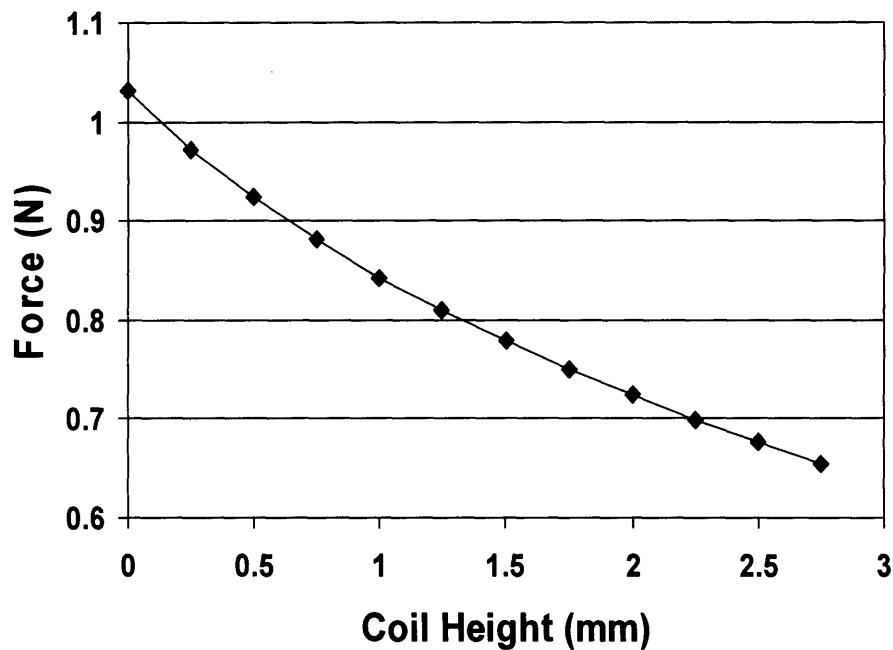


**FIGURE 31:** Force vs. the height of the coil above the magnet for constant current and channel parameters

This graph in Figure 31 shows a slightly off linear relation between force and coil height. The reason for this nonlinearity is because while the magnetic flux concentration decreases with height, the direction of the flux lines becomes more horizontal at increased heights.

The deflection per current ratio for the 6.35mm channel width is 0.5% smaller than the 3.18mm channel. This does not fit our model; it should be that no force can be lost by increasing the channel width. This is likely due to the voltage shift in the capacitance probe. As the results were being recorded from the first data point to the last a shift of about 0.4V was recorded. This varied depending on the time it took to record each experimental set as well as the number of different currents run in each set.

The capacitance probe measures the deflection. In each experiment it was necessary to readjust the cap probe. If the cap probe was fitted at a slight angle it would read a different displacement than if it were perfectly straight. This would increase the deflection per current ratio of that particular run.

# Chapter 7: Conclusions

## 7.1 Purpose

The purpose of this thesis was to show that by adding a flux channel to a planar magnet-coil actuator the input to output efficiency could be augmented. Further, that the effectiveness of the channel depends on channel width and an equation can be found to define the relationship.

The growing MEMS device technology and applications requires more innovative research be done on improving the space and power efficiency of the devices. The more mechanical force that can be generated for a given electrical input, the stronger the device.

The characterization of magnetic fields in the presence of metal interference or channeling was not well defined. For the furtherance of MEMS research it was beneficial to model flux channels for actuator systems.

## 7.2 Solution

This work has aided in the characterization of channeling effects on magnetic fields by suggesting a relationship between actuator deflection and the flux channel geometry. The relationship suggested by simulation is

$$\delta = 0.1478\text{mm} + 0.0102\text{mm} (1 - \exp(-2.6W/\text{mm}))$$

where the deflection,  $\delta$ , is related as a function of the channel width,  $W$ . This relationship is specific to the dimensions of the magnet used in this experiment.

## 7.3 Validity of solution

The experiment showed that the width of the channel relates as predicted in the simulation to the actuator output. The curve above is valid up to a critical channel width at which the added output becomes constant. The added deflection from the flux channel in the experiment was 46.7% and in the simulation the deflection was augmented 48.8%. This shows that the model proposed is correct to 4.3% of the deflection.

These principles all scale with overall size of the system. If the system were downsized to a micro-scale as an actuator would be in a MEMS device, these relationships will still hold. This principle of the addition of a channel can be used in further designs of planar magnet-coil actuators. The flux channel also provides a safe packaging for the actuator, a current need in growing MEMS technology.

# Chapter 8: References

[01] Freedman, Roger A., Hugh D. Young, *University Physics Vol. 2*, 9<sup>th</sup> Edition, pp. 866-873, Addison Wesley Publishing Company, Inc., 1996.

[02] Kim, Ki Hoon, Hyeun Joong Yoon, Ok Chan Jeong, Sng Sik Yang, *Sensors and Actuators, A 117*, pp. 8-16, "Fabrication and test of a micro electromagnetic actuator", 2005.

[03] Crandall, Stephen H., Norman C. Dahl, Thomas J. Lardner, *An Introduction to the Mechanics of Solids*, Second Edition with SI Units, pp. 416-422, McGraw-Hill Book Company, New York, 1976.

# Appendix

## A.1 Force vs. current simulations

Figures 32 and 33 display the results from the Ansoft electro-magnetic simulations for the two different channel widths. Figure 32 shows a linear relation between output force and input current of 0.3537N/A for the channel width of 6.35mm. Figure 33 shows a linear relation between output force and input current of 0.3544N/A for a channel width of 9.53mm.

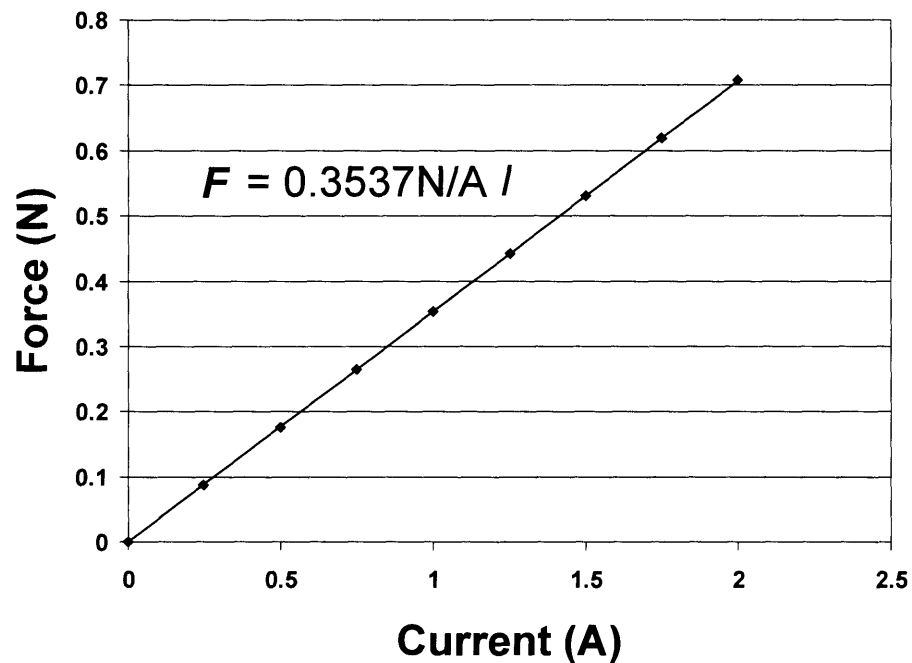


FIGURE 32: Force vs. current for channel width of 6.35mm

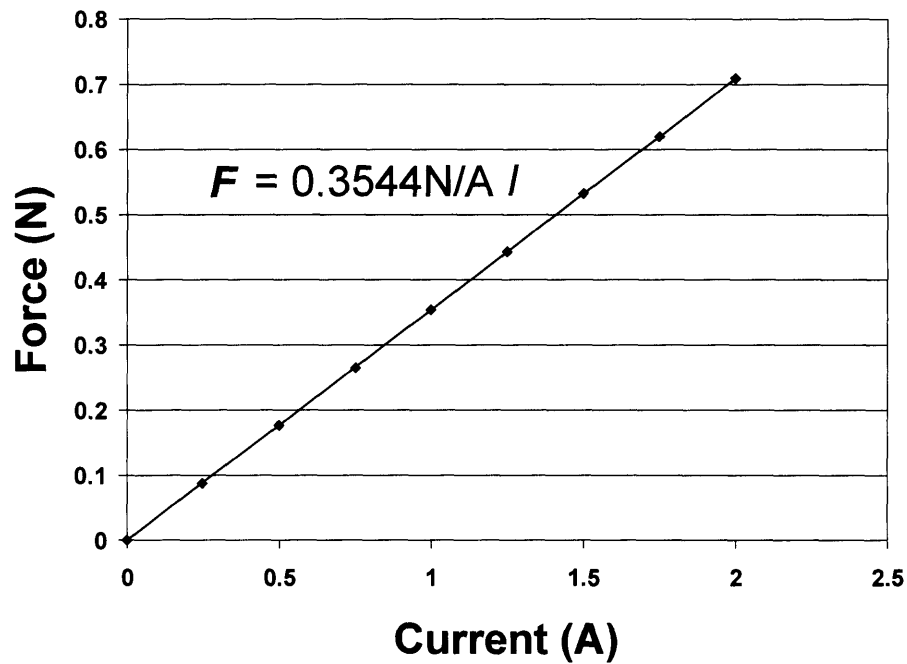
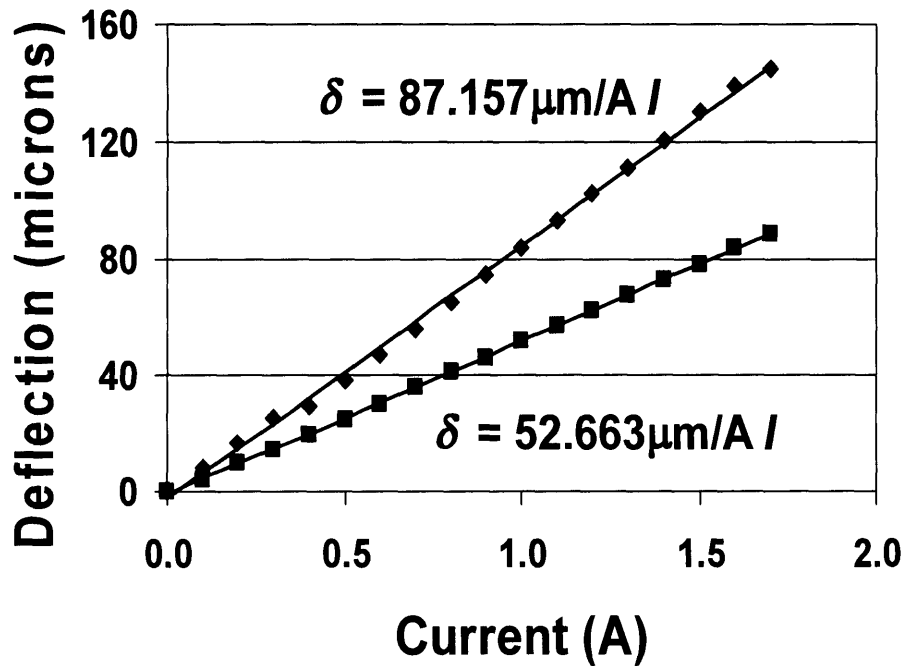


FIGURE 33: Force vs. current for channel width 9.53mm

### A.2 Experimental results

Figures 34 through 37 are the results gathered in the experiment. Figure 34 shows the relationship between deflection of the actuator in microns to the input current for the channel width of 3.18mm and 0mm.





**FIGURE 34:** Deflection vs. current for 3.18mm channel width (top) and 0mm channel width (bottom)

Figure 35 shows the relationship between deflection in microns and current for the channel width of 9.53mm. The channel base thickness was set at 3.18mm as described in the experimental procedure.

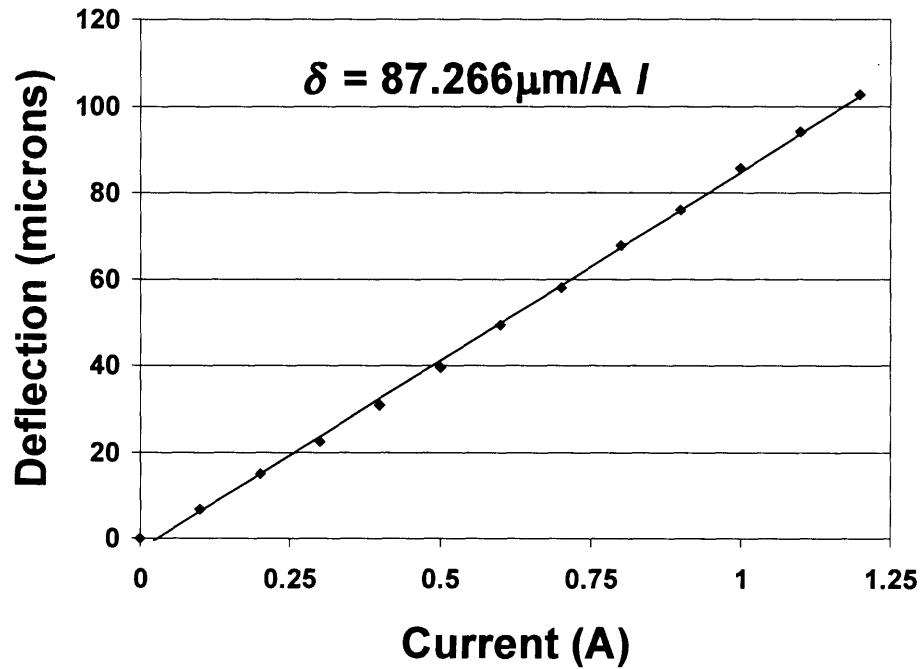


**FIGURE 35:** Deflection vs. current for channel width of 9.53mm

Figures 36 and 37 show the relationship between deflection and current for the channel widths of 0mm and 6.35mm. The linear relationships were used in compiling the composite results in Figure 27 and 28.

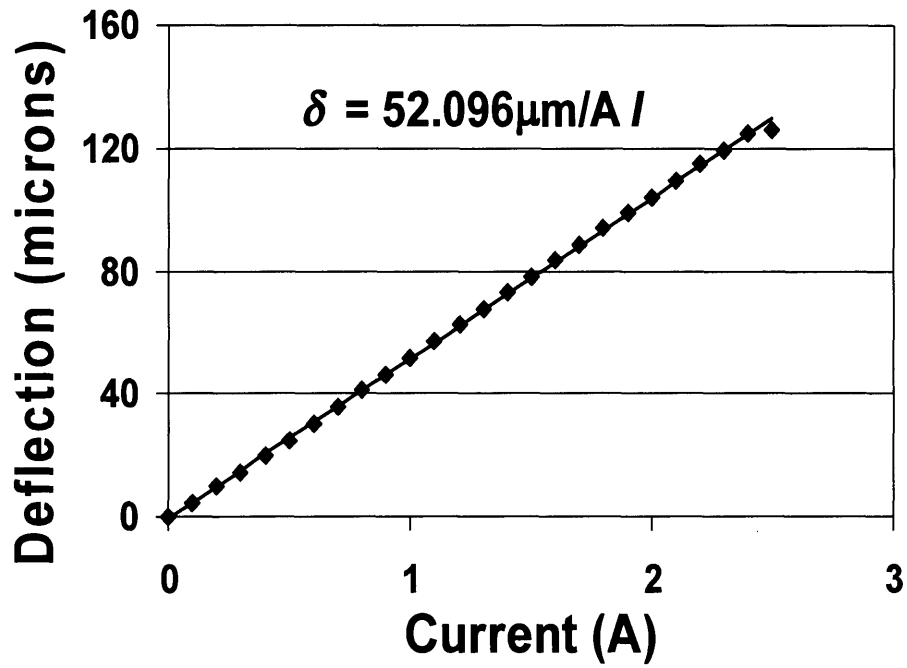


FIGURE 36: Deflection vs. current for channel width of 0mm but with a 2.7mm channel base thickness

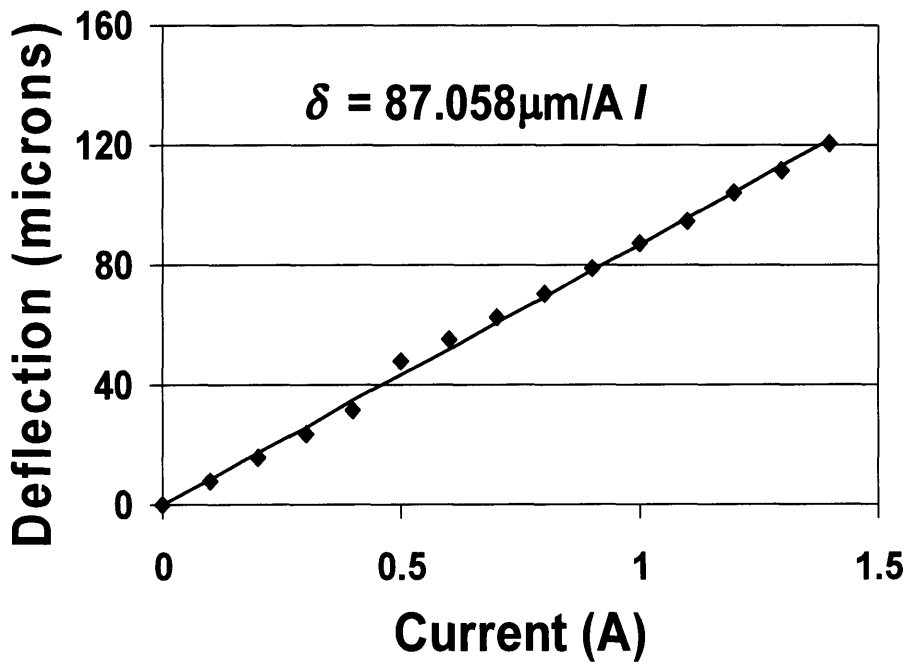


FIGURE 37: Deflection vs. current for the channel width of 6.35mm